



UNIVERSITY OF LEEDS

This is a repository copy of *Development of an automated underwater abrasion rig to determine galvanic effects during the growth and localised breakdown of surface films in CO<sub>2</sub>-containing solutions*.

White Rose Research Online URL for this paper:  
<http://eprints.whiterose.ac.uk/143141/>

Version: Accepted Version

---

**Article:**

Barker, R [orcid.org/0000-0002-5106-6929](https://orcid.org/0000-0002-5106-6929), Yazdi, R, Hua, Y et al. (5 more authors) (2019) Development of an automated underwater abrasion rig to determine galvanic effects during the growth and localised breakdown of surface films in CO<sub>2</sub>-containing solutions. *Review of Scientific Instruments*, 90 (3). 034101. ISSN 0034-6748

<https://doi.org/10.1063/1.5064850>

---

© 2019 Author(s). This is an author produced version of a paper accepted for publication in *Review of Scientific Instruments*. Uploaded in accordance with the publisher's self-archiving policy.

**Reuse**

Items deposited in White Rose Research Online are protected by copyright, with all rights reserved unless indicated otherwise. They may be downloaded and/or printed for private study, or other acts as permitted by national copyright laws. The publisher or other rights holders may allow further reproduction and re-use of the full text version. This is indicated by the licence information on the White Rose Research Online record for the item.

**Takedown**

If you consider content in White Rose Research Online to be in breach of UK law, please notify us by emailing [eprints@whiterose.ac.uk](mailto:eprints@whiterose.ac.uk) including the URL of the record and the reason for the withdrawal request.



[eprints@whiterose.ac.uk](mailto:eprints@whiterose.ac.uk)  
<https://eprints.whiterose.ac.uk/>

**Development of an automated underwater abrasion rig to determine galvanic effects during the growth and localised breakdown of surface films in CO<sub>2</sub>-containing solutions**

Richard Barker\*, Rouhollah Yazdi, Yong Hua, Andrew Jackson, Ali Ghanbarzadeh, Mick Huggan, Thibaut Charpentier and Anne Neville

Institute of Functional Surfaces, School of Mechanical Engineering, University of Leeds, LS2 9JT.

\* Corresponding author: R.JBarker@leeds.ac.uk

**Abstract**

This paper outlines the development of an automated underwater abrasion rig to assist in understanding the galvanic interaction induced by surface films when continuous localised mechanical film breakdown is encountered on the surface of carbon steel in CO<sub>2</sub>-containing environments. The rig enables the measurement of galvanic current between a small X65 steel pin and a larger steel specimen, as well as the intrinsic corrosion rate of an additional, uncoupled larger specimen. The surface film developed on the pin is removed periodically using an automated reciprocating and rotating shaft with a sand paper grit pad attached to the base, while the surface film is allowed to establish itself undisrupted on the large specimen. The setup essentially simulates a tribo-corrosion process where local removal of material occurs within a carbon steel pipeline as a result of periodic sand particle impingement. Initial results focus on validating the reproducibility of the technique, as well as determining the galvanic effects associated with iron carbide and iron carbonate for two model sets of conditions to highlight the capabilities of the system.

## 1.0 Introduction

Localised carbon dioxide ( $\text{CO}_2$ ) corrosion of carbon steel remains one of the most aggressive forms of corrosion within the oil and gas industry<sup>[1]</sup>. The rate of local material loss experienced by steel pipelines can be very difficult to predict and orders of magnitude greater than the overall uniform corrosion rate. A number of environmental, operational and metallurgical factors have been attributed to the onset of mesa-attack in carbon steel pipelines. These include poor chemical inhibition, local flow disturbances, bacteria, organic acids and hydrogen sulphide ( $\text{H}_2\text{S}$ ) amongst others<sup>[2-8]</sup>. Considering the number of factors conducive to mesa-attack, this form of degradation is notoriously difficult to both predict and quantify.

Under  $\text{CO}_2$ -containing conditions, a variety of different surface films can develop on carbon steel; the most common of these include iron carbide ( $\text{Fe}_3\text{C}$ ) and iron carbonate ( $\text{FeCO}_3$ )<sup>[9-11]</sup>.  $\text{Fe}_3\text{C}$  layers are produced through the dissolution of the ferrite phase within carbon steels (i.e. they are already part of the steel microstructure and the layer is revealed further as a result of the selective dissolution process)<sup>[9]</sup>. The development of porous  $\text{Fe}_3\text{C}$  films has been shown to accentuate the uniform corrosion rate of carbon steels through acceleration of the cathodic hydrogen evolution reaction in  $\text{CO}_2$  environments (due to its ability to provide a lower over-potential compared to the ferrite phase)<sup>[12]</sup>. The precipitation of  $\text{FeCO}_3$ , however, has the ability to slow down the corrosion process at the steel interface by creating a diffusion barrier and/ or blocking active sites on the steel surface<sup>[13-16]</sup>. The protective nature of this crystalline film and its precipitation rate are influenced by a number of factors such as temperature, microstructure,  $\text{CO}_2$  partial pressure, and the supersaturation of  $\text{FeCO}_3$  within the system<sup>[10]</sup>. It is believed that when such protective layers form and are locally disrupted, the initiation and propagation of localised corrosion can result, which lead to the failure of pipelines<sup>[17-20]</sup>.

The breakdown of  $\text{FeCO}_3$  films has been the subject of extensive discussion in the literature and can occur via mechanical effects<sup>[18]</sup>, chemical dissolution<sup>[20]</sup> or a combination of both processes<sup>[19]</sup>. A handful of studies have suggested that following the breakdown of an  $\text{FeCO}_3$  film, a galvanic cell is created between the covered and uncovered areas of the steel<sup>[1,21]</sup>. The work presented in this study is directed towards building upon such previous research through the design and testing of an underwater abrasion device.

This unique setup enables the level of galvanic interaction at different stages of the corrosion process to be observed, providing a deeper insight into the evolution of the localised corrosion mechanism.

## **1.1 Previously developed test cells and methodologies to evaluate localised corrosion**

Prior to introducing the automated underwater abrasion rig setup, it is perhaps prudent to review other tests cells developed to understand localised corrosion within the literature in order to highlight the unique abilities of this system. Therefore, such test cells are summarised within the preceding paragraphs.

### **1.1.1 The 'pencil pit' method**

One particular method which has proved popular for evaluating localised corrosion/ pit propagation in CO<sub>2</sub> environments is the so called 'artificial pit' or 'pencil pit' technique<sup>[1, 22, 23]</sup>. The system consists of a large carbon steel cathode and a small diameter (1 to 2 mm) anodic 'pit' sample of the same material which is positioned ideally in the centre or in close proximity to the large sample (to minimise ohmic resistance in the aqueous phase) and isolated in the solution using resin or Polyether ether ketone (PEEK). The anode and cathode are galvanically connected externally from the cell using a potentiostat and monitored using a zero-resistance ammeter (ZRA). In some instances, researchers have made the depth of the anode adjustable to simulate different stages of pit propagation, although it is debatable how representative such a scenario is of a truly natural pit.

The pencil pit technique essentially tries to replicate a system where either the film breakdown is chemical or a where a pit generates due to the inherent inhomogeneous nature of the film. Examples of the application or variations on this galvanic coupling technique include work by Marsh et al.<sup>[22]</sup> and Turnbull of al.<sup>[23]</sup> to evaluate localised corrosion propagation in CO<sub>2</sub> environments in the presence of inhibitors, Amri et al.<sup>[6, 7]</sup> to investigate pit growth in carbon steel in the presence of acetic acid, and by both Han et al.<sup>[1]</sup> and Fernandez-Domene et al.<sup>[21]</sup> to evaluate the propensity for localised corrosion/ pits to propagate in environments where the formation and disruption of protective FeCO<sub>3</sub> films are possible.

Fernandez-Domene et al.<sup>[21]</sup> established that galvanic effects can exist between the bare steel and an FeCO<sub>3</sub> covered surface. They identified that the magnitude of the galvanic current density was influenced by the anode to cathode area ratio. Tests performed at 60°C and pH 5.5 produced galvanic interactions between 3.8±0.12 to 263.0±43 μA/cm<sup>2</sup> for cathode:anode area ratios from 1:1 to 200:1, respectively.

In a separate study, Han et al.<sup>[1]</sup> utilised the artificial pit technique to understand the CO<sub>2</sub> environments and/or operating conditions which were conducive to localised attack. They identified that the galvanic interaction between the bare steel and FeCO<sub>3</sub> filmed steel was driven by the potential difference between the two areas and as a consequence, local attack could only be sustained by maintaining this potential difference. Based on these observations, Han et al.<sup>[1]</sup> suggested that a unique set of conditions need to be established whereby no significant dissolution nor precipitation can be expected once a protective film had formed and been disrupted. This was estimated to be within the FeCO<sub>3</sub> supersaturation range of 0.5 to 2.

### 1.1.2 The 'scratch' test

One method by which protective layers on carbon steel surfaces such as FeCO<sub>3</sub> can be removed is through the impingement of sand particles. In multiphase flow environments with sand particles, competition will exist between the removal of the protective film by mechanical erosion and the rate at which the film heals. If the removal rate of the film is greater than the formation rate, then accelerated corrosion rates will exist in the area of removal, purely through differences in the intrinsic corrosion rates at each location. In addition, galvanic interactions may occur locally within the vicinity of the removal region, accentuating the corrosion rate even further. Such a process is essentially an erosion-corrosion or tribo-corrosion mechanism involving galvanically enhanced dissolution, which has the potential to lead to excessive localised corrosion rates.

One method to understand and model this process is to use a 'scratch test' experimental setup. These experiments have been conducted by McMahon and Martin<sup>[24]</sup> to evaluate the effects of mechanical damage on corrosion resistant alloys, as well as Rincon et al.<sup>[25, 26]</sup> to evaluate the erosion-corrosion resistance of 13Cr alloy as a function of solution pH and temperature in CO<sub>2</sub> environments. Based on a review of the literature, the scratch test methodology appears to have only been implemented on passive materials which establish a protective chromium oxide layer. The setup of the system is essentially the

same as the pencil pit method, however, the anode and cathode have to be fully separated in this instance (as opposed to the anode being isolated in the centre of the cathode). The small anode pin is positioned underneath a grinding disc. Once protective passive films are established on both the large cathode and small anode, the grinding pad is lowered onto the anode pin to abrade the passive film away. The mixed potential and galvanic current between the two working electrodes are then monitored to identify how quickly the protective film re-establishes itself on the anode. The grinding process made on a well-defined pin area may be interpreted as similar to the removal of the passive layer due to particle impact; hence this system can be used to understand the accentuation of corrosion locally on the alloy surface as a result of the mechanical removal process.

The research conducted in the present study focuses on building upon the previous work of the aforementioned authors by implementing an automated abrasion system (or automated scratch test) to look at the implications of continuous removal of surface layers on carbon steel in CO<sub>2</sub> environments and how the galvanic current manifests itself over time during film growth on the cathode. This essentially replicates an erosion-corrosion environment whereby a surface film (Fe<sub>3</sub>C, FeCO<sub>3</sub> or otherwise) is completely prevented from ever properly establishing itself locally on a section of pipework. By continually disrupting the film, a scenario will be modelled in which the maximum possible localised corrosion can occur due to erosion-corrosion conditions. This will help to better understand systems with controlled experimental variables.

## **2.0 Experimental Procedure**

This section introduces the design of the underwater abrasion rig, before outlining the test matrix and specimen preparation.

### **2.1 Development and setup of the underwater abrasion rig**

The underwater abrasion system is depicted through the schematic shown in Figure 1. The setup consists of a sample holder (which contains two 4.9 cm<sup>2</sup> X65 samples as well as a 0.0314 cm<sup>2</sup> X65 pin), a motor (to control rotation of the grinding pad), a solenoid (to apply a pre-calibrated load to the X65 pin surface using a grinding pad during abrasion) and the grinding pad itself (to abrade the surface with a chosen grade of 1200 silicon carbide (SiC) grit paper). In addition, various support shafts and mounting plates are

provided for stability, as well as springs to facilitate retraction of the grinding pad once the load is finished being applied.

The system allows the user to follow the effect of corrosion product formation on the total dissolution rate of the steel under different conditions whilst also measuring galvanic interactions between the filmed portion of the steel and the small, exposed bare steel pin. Such a process can identify whether local disruption to a corrosion product layer is capable of establishing significant galvanic effects which may be able to result in localised corrosion.

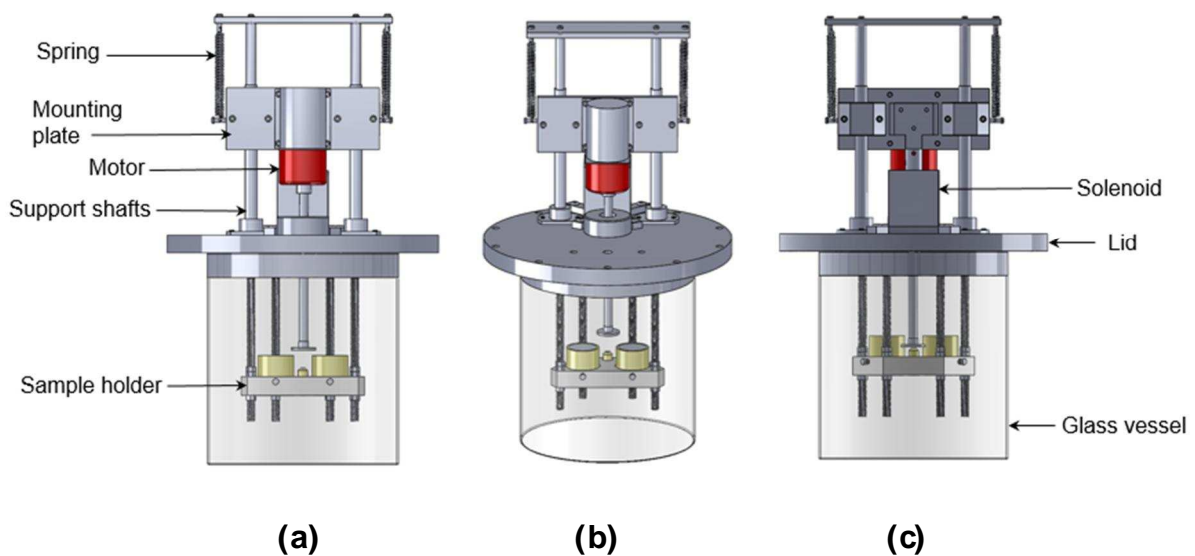


**Figure 1: Schematic of under-water abrasion rig (a) front view; (b) isometric view; and (c) rear view.**

## **2.2 Sample configuration, electrochemical measurements and abrasion process**

The test samples consist of a small X65 carbon steel pin ( $0.0314 \text{ cm}^2$  exposed area) and two large X65 steel specimens ( $4.9 \text{ cm}^2$  area each). Wires were soldered to the back of each sample and embedded in a non-conducting resin. The pin was machined and embedded into resin in a particular shape to ensure consistent scratch geometries after every abrasion process and ensure minimal abrasion of the resin. It was also positioned within very close proximity to the larger sample to which it was coupled to, in order to minimise ohmic resistance in the aqueous phase. For all samples, only one surface of the electrode was exposed to the solution, with the other sides all being covered with epoxy

resin. The sets of samples and arrangement within the sample holder is shown in Figure 2.

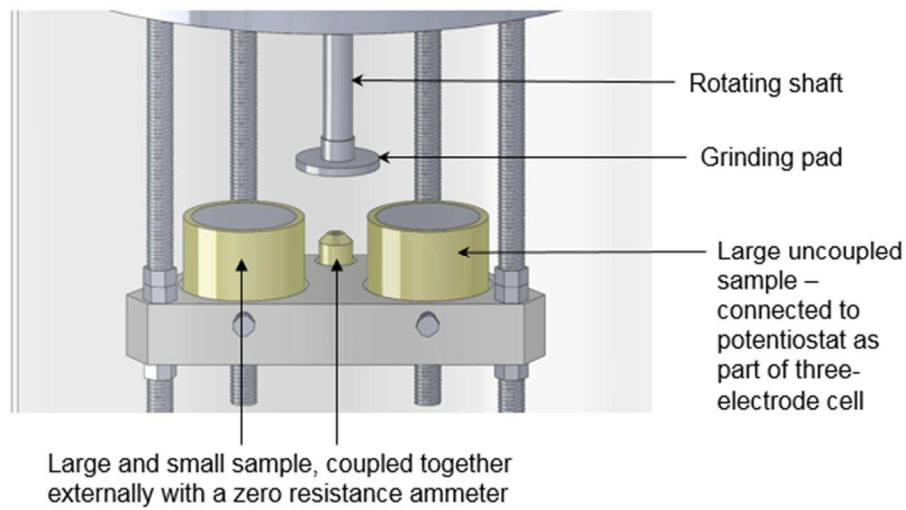


**Figure 2: Schematic of sample configuration for LPR and galvanic measurements of X65 steel electrodes in the abrasion rig**

One of the 4.9 cm<sup>2</sup> specimens was linked to one channel of a multi-channel potentiostat and forms the working electrode in a three-electrode cell arrangement which includes a platinum counter electrode and a silver/ silver chloride (Ag/ AgCl) reference electrode. The linear polarisation resistance (LPR) technique was applied to this sample to determine the intrinsic corrosion rate response with time. This consisted of polarising the working electrode from -15 mV vs the open circuit potential (OCP) to +15 mV vs OCP at a scan rate of 0.25 mV/ s once every hour. The polarisation resistance determined from the technique was corrected for solution resistance (determined from AC measurements) to produce a charge-transfer resistance ( $R_{ct}$ ) which was subsequently converted into a corrosion current density using the Stern-Geary relationship (Equation (1)):

$$i_{corr} = \frac{B}{R_{ct}} = \frac{1}{R_{ct}} \frac{\beta_a \beta_c}{2.303(\beta_a + \beta_c)} \quad (1)$$

where  $B$  is the Stern-Geary coefficient,  $\beta_a$  is the magnitude of the anodic Tafel constant and  $\beta_c$  is the magnitude of the cathodic Tafel constant (determined in separate experiments). The value of  $i_{corr}$  was then used in conjunction with Faraday's Law and an appropriate conversion factor (Equation (2)) to obtain the corrosion kinetics in mm/ year.

$$CR = \frac{Ki_{corr}M_{Fe}}{nF\rho} \quad (2)$$

where K is a conversion factor to obtain corrosion rate (CR) in units of mm/ year ( $K = 3.16 \times 10^5$ ),  $M_{Fe}$  is the molar mass of iron (55.8 g), n is the number of electrons freed in the corrosion reaction (2 electrons),  $\rho$  is the density of steel ( $7.87 \text{ g/ cm}^3$ ) and F is the Faraday constant (96,485 coulomb/ mole)

The second channel of the potentiostat was used to provide an external couple between the small X65 pin and the second large X65 sample through a zero resistance ammeter (ZRA), with the samples being coupled from the very beginning of the experiment. This facilitates real-time measurements of the current exchange as well as the mixed potential relative to a Ag/ AgCl reference electrode. The technique enables the galvanic interaction between the small abraded pin and the larger filmed sample to be quantified.

The potentiostat used for the experiments (ACM Instruments Gill AC), operates sequentially, with only one channel in operation at any given point in the experiment. For these particular experiments, the sequence of measurements chosen is provided in Figure 3. Initially, an LPR measurement is performed on the large uncoupled sample, lasting approximately 2 minutes. The potentiostat then switches to the second channel and records both the mixed potential and galvanic current exchanged between the two coupled samples (one measurement every 5 seconds for ~58 minutes). Approximately 500 seconds into the galvanic measurement, the abrasion process of the small X65 pin occurs.

The abrasion process was controlled through the use of a simple Labview program which was synchronised with the software employed by the potentiostat. The Labview programme initiates the motor to run at 250 rpm prior to engaging the solenoid for 3 seconds, placing the 1200 SiC grinding pad onto the surface of the X65 steel pin. The power to the solenoid is then cut and the grinding pad is retracted using the spring system prior to the rotation of the shaft ceasing. The process is repeated every hour in the experiments presented here for 60 hours. It is important to note here that this process was evaluated in terms of its sensitivity to abrasion time and load, with no sensitivity to the behaviour of the sample being shown beyond 3 seconds of contact or at any of the loads capable of being applied within the system.

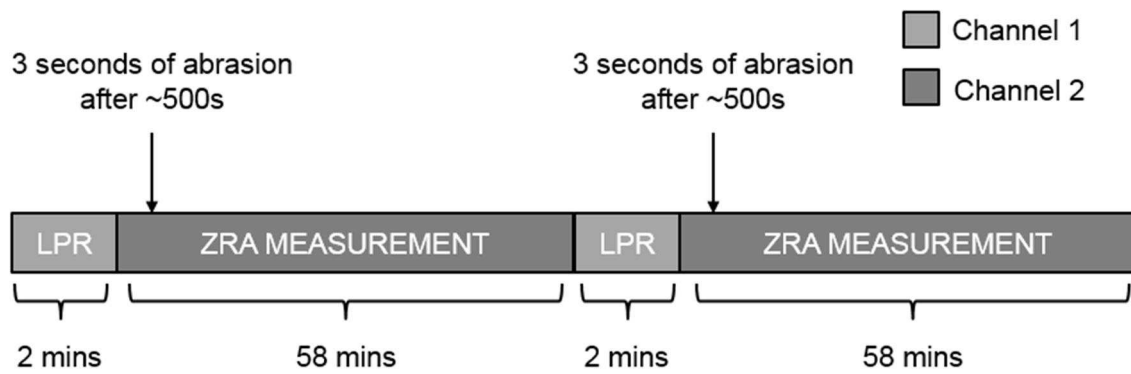


**Figure 3: Measurement and abrasion sequence performed by the potentiostat and Labview program during experiments; the cycle shown was repeated over the entire duration of the experiment.**

### 2.3 Materials and solution preparation

All working electrodes were made from API 5L X65 steel with the composition provided in Table 1. The steel possesses a ferritic-pearlitic microstructure as shown in the optical microscope image in Figure 4. Prior to every experiment, samples were wet-ground with SiC papers up to 1200 grit finish.

**Table 1: Elemental composition (wt.%) of API 5L X65 carbon steel**

C	Si	Mn	P	S	Cr	Mo	Fe
0.12	0.18	1.27	0.008	0.002	0.11	0.17	Balance

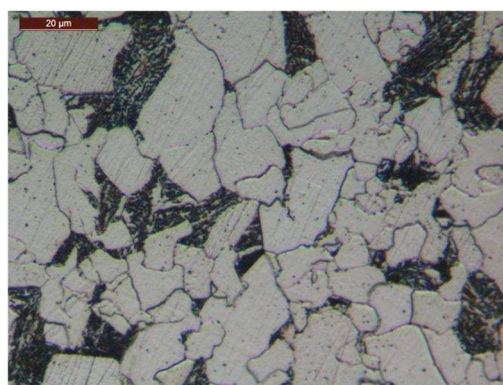


**Figure 4: Microstructure of API 5L X65 depicting a ferritic-pearlitic structure; Surface preparation consisted of polishing the surface using 3 μm diamond suspension to attain a mirror finish, followed by etching in a 2% nital solution for 10 to 20 seconds**

All experiments were conducted in a glass vessel containing 2 litres of 3.5 wt.% NaCl brine which was fully saturated with CO<sub>2</sub> at atmospheric pressure. The pH of the solution was adjusted if required using sodium bicarbonate. CO<sub>2</sub> was bubbled into the test solution for at least 4 hours prior to performing the experiment, as well as continuously throughout the test to ensure complete saturation. The rate of bubbling was carefully controlled to ensure no hydrodynamic disruption to the steel surface. The two preliminary tests conducted within this paper are outlined in Table 2. The purpose of these test conditions was to develop two distinctly different surface layers on the carbon steel surface to evaluate their galvanic effects. Test Environment 1 in Table 2 would predominantly create a Fe<sub>3</sub>C layer (low temperature and low pH), whilst Test Environment 2 would result in the gradual growth of an FeCO<sub>3</sub> film (high temperature and high pH).

**Table 2: Experimental conditions evaluated using the underwater abrasion rig**

Parameter	Test environment 1	Test environment 2
Brine chemistry	3.5 wt.% NaCl	
Temperature	30°C	70°C
Initial pH	~3.8	~6.8-6.9
pCO <sub>2</sub>	0.96 bar	0.69 bar

The morphology of the corrosion products was examined using a Carl Zeiss EVO MA15 scanning electron microscope (SEM) at the end of each experiment. All SEM images were collected at an accelerating voltage of 20 kV and at a working distance of around 8 mm.

### 3.0 Results and discussion

#### 3.1 Test Environment 1 – development of Fe<sub>3</sub>C film

##### 3.1.1 Corrosion rate behaviour of uncoupled sample

Figure 5 shows the corrosion rate and open circuit potential (OCP) behaviour of X65 steel over 60 hours at 30°C in a CO<sub>2</sub>-saturated 3.5 wt.% brine at pH 3.8. A gradual increase in corrosion rate is observed from ~1.1 to 1.4 mm/year in conjunction with a rise in OCP by 30 to 40 mV over 60 hours. Such behaviour can be attributed to the revealing of a Fe<sub>3</sub>C network as a result of preferential dissolution of the ferrite phase within the steel

microstructure and accentuation of the cathodic hydrogen evolution reaction<sup>[12, 27]</sup>. The ability of Fe<sub>3</sub>C to enhance the corrosion rate of the steel lies in its conductive nature and the fact it is able to increase the rate of the cathodic reaction, through either the process of internal acidification, galvanic effects or a combination of both<sup>[9, 12]</sup>. Such effects have been reported by numerous authors under CO<sub>2</sub>-containing environments where the formation of protective corrosion product layers does not occur<sup>[2, 3, 27-31]</sup>. The difference between the OCP of the Fe<sub>3</sub>C-rich surface at the end of the experiment and the bare steel surface at the beginning of the experiment suggests that a galvanic cell is capable of being established between the two surfaces.

The SEM images provided in Figure 6(a) and (b) indicate that there has been preferential dissolution of the ferrite phase within the steel microstructure. Ferrite-rich areas have receded and the ferrite-containing regions within the pearlite lamella structure have also preferentially dissolved. The corresponding x-ray diffraction pattern of the specimen in Figure 6(c) indicates the presence of Fe<sub>3</sub>C on the steel surface.

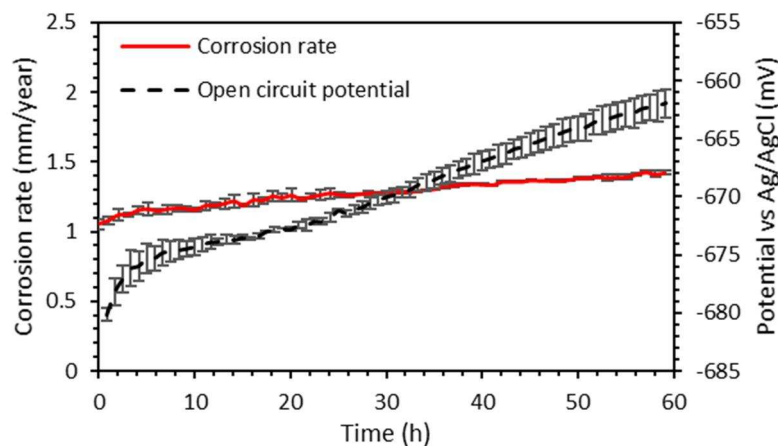
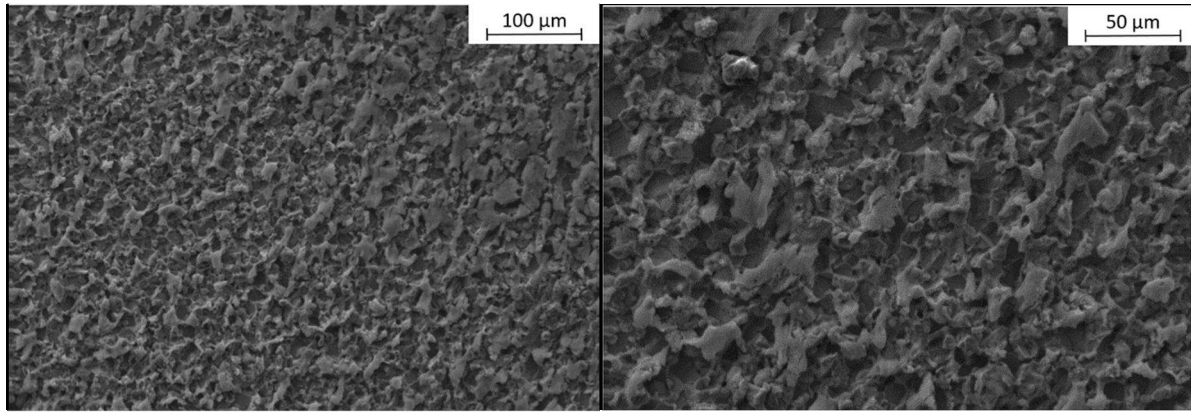
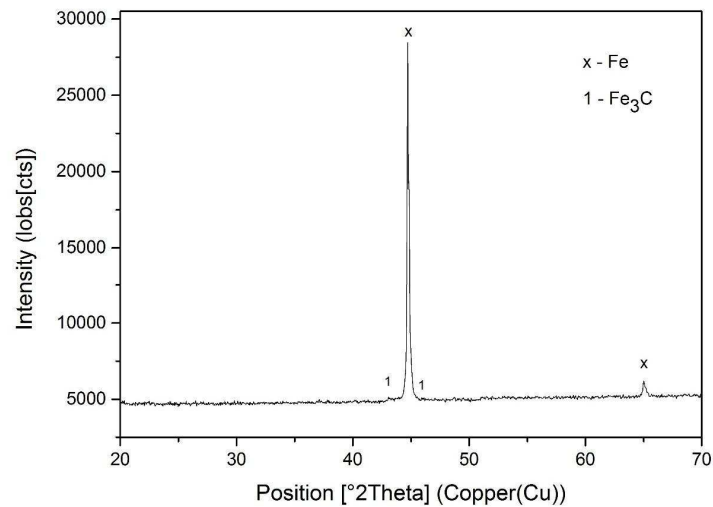


**Figure 5: Corrosion rate and open circuit potential of X65 carbon steel exposed to a CO<sub>2</sub>-saturated 3.5 wt.% NaCl solution at 30°C and pH 3.8 for 60 hours. A Stern-Geary coefficient of 14 was used to convert the charge-transfer resistance into corrosion rate.**



(a)

(b)



(c)

**Figure 6: SEM images of X65 carbon steel exposed to a CO<sub>2</sub>-saturated 3.5 wt.% NaCl solution at 30°C and pH 3.8 for 60 hours at (a) lower and (b) higher magnification, as well as (c) the corresponding diffraction pattern from the specimen surface**

### 3.1.2 Galvanic current and mixed potential behaviour of coupled samples

Figures 7(a) to (c) show the galvanic interaction between the repeatedly abraded pin (noting that it is abraded once every hour for 3 seconds) of area 0.0314 cm<sup>2</sup> and the larger sample on which the Fe<sub>3</sub>C film is allowed to evolve over 60 hours without any disruption. This interaction is displayed in the form of a mixed potential between the two samples and their galvanic current density measured using a ZRA (with a positive current signifying the pin as the anode within the galvanic couple).

For clarity, key stages in the evolution of the galvanic interaction between the pin and the large sample are shown over the 60 hour period in Figures 7(a) to (c). The galvanic transient responses consist of galvanic cycles which comprise of peaks (coinciding with the onset of the abrasion process), followed by a current decay (noting that the galvanic current densities are represented based on the area of the small pin). In addition, a mixed potential is provided, with the potential being dominated by that of the larger sample in this instance. This was confirmed in separate experiments where the uncoupled potential of both specimens was monitored, and after each abrasion, the OCP of the pin was shown to remain within a few mV of the starting potential of the larger sample. Such observations are sensible given that the surface is returned to its original wet-ground state after each abrasion processes.

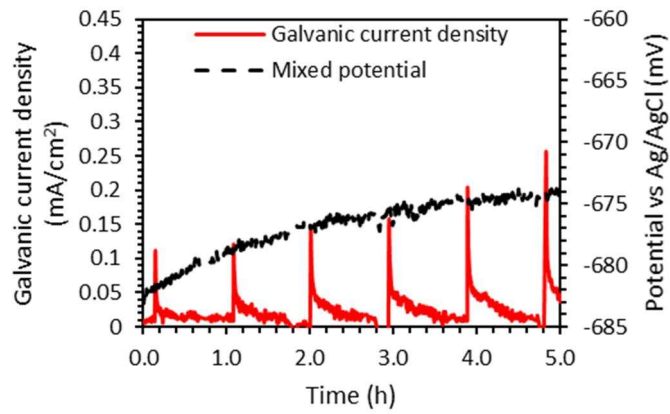
As shown in Figure 7(a), during the early stages of the experiment, the galvanic current exhibits a sharp rise in the positive current, followed by a decay for each one hour cycle. The potential difference between the large sample and the abraded pin gives rise to the observed current response. The potential difference is such that the large sample establishes itself as the net cathode within the galvanic couple, resulting in the pin becoming a net anode, causing it to corrode faster than its intrinsic corrosion rate. After each abrasion process in Figure 7(a), the galvanic current peaks and decays back to values close to 0 mA/cm<sup>2</sup> by the end of each one hour cycle, presumably related to the diminishing potential difference between the two samples with time as Fe<sub>3</sub>C evolves on the pin. Over the time period shown in Figure 7(a), the average galvanic current density is 0.036 mA/cm<sup>2</sup> which equates to ~0.4 mm/year accentuation of the carbon steel pin from its initial intrinsic corrosion rate of ~1.1 mm/year in this environment.

As the mixed potential increases throughout the duration of the experiment, the potential difference between the abraded pin and the large sample inevitably becomes larger at the start of each cycle (recalling that the OCP of the pin returns to a very similar potential after every abrasion process, whilst the potential of the large sample is allowed to evolve). This is demonstrated in Figure 7(b) between 30 and 35.5 hours where the mixed potential is ~10 mV greater than that at the beginning of the experiment (noting again that the mixed potential is dominated by the larger sample). Owing to the greater potential difference as a result of the more established Fe<sub>3</sub>C layer on the larger sample, the galvanic current is unable to 'recover' within the 1 hour cycle, producing a positive

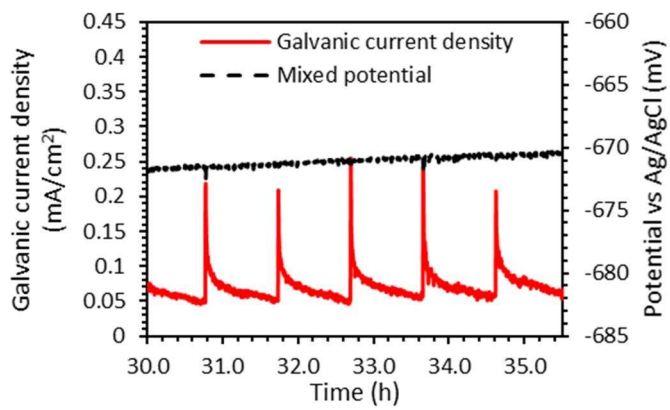
current which fails to fully decay to zero. Over the period of 30 to 35.5 hours, the average galvanic current is  $0.070 \text{ mA/cm}^2$  ( $\sim 0.8 \text{ mm/year}$ ). This means that the galvanic effect has almost doubled the corrosion rate of the carbon steel pin from that of its initial intrinsic corrosion rate by this stage of the experiment.

Figure 7(c) shows the galvanic response towards the end of the 60 hour experiment (54 to 59.5 hours). Again, an increase in the mixed potential and galvanic current density is recorded. The potential has risen by 15 to 20 mV from that at the start of the experiment, and the galvanic current fails to fall below  $0.15 \text{ mA/cm}^2$  with an average current of  $0.195 \text{ mA/cm}^2$  ( $2.3 \text{ mm/year}$ ) produced. It is clear from the behaviour over the course of the experiment that the OCP difference between the two specimens drives a significant galvanic current. The total corrosion rate of the anodic pin can be thought to consist of the intrinsic corrosion rate plus the galvanic contribution. Therefore, over the course of the cycles between 55 and 59.5 hours, the average corrosion rate in this experiment (including the galvanic contribution) is  $3.4 \text{ mm/year}$ , which is three times that of the corrosion rate if the pin were to be uncoupled under these conditions. This provides proof that local galvanic cells can be established between a large  $\text{Fe}_3\text{C}$ -rich surface and a small bare steel surface, and that localised corrosion can propagate when a stable difference in potential between the two is established.

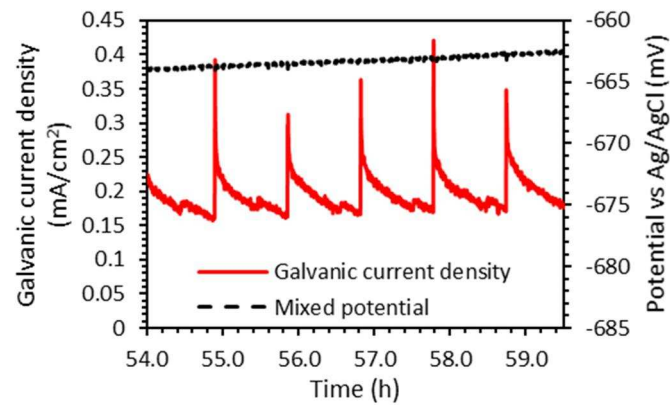
The results show that this technique is able to determine the galvanic interaction between a continuously, locally eroded region of carbon steel, and a larger nearby area with a continuously evolving  $\text{Fe}_3\text{C}$  layer on the steel surface. Through repetitive abrasion of the small X65 pin, it is possible to determine how the evolution of  $\text{Fe}_3\text{C}$  on the steel surface influences the magnitude and recovery rate of the galvanic response, which are both important factors when identifying the threat of localised corrosion within an erosion-corrosion  $\text{CO}_2$  environment.



(a)



(b)



(c)

**Figure 7: Galvanic current and mixed potential as a function of time for an X65 steel pin connected to a larger X65 sample, where the steel pin is abraded repetitively every hour for 3 seconds and the large sample is left to corrode. Test conditions are a CO<sub>2</sub>-saturated 3.5 wt.% NaCl solution at 30°C and pH 3.8 for 60**

**hours; (a) time period of 0 to 5.5 hours; (b) time period of 30 to 35.5 hours and (c) time period of 54 to 59.5 hours displayed for clarity.**

Figures 7(a) to (c) shows in stages that as the mixed potential rises throughout the course of the experiment (in accordance with the evolution of  $\text{Fe}_3\text{C}$  on the larger steel sample), so too does the magnitude of the galvanic current between the small pin and the larger sample. In fact, the two properties rise almost concomitantly with one another over the duration of the experiment.

To illustrate the overall response more clearly, Figure 8 shows the intrinsic corrosion rate of the pin at selected one-hour time periods (which is assumed to be relatively stable due to repeat abrasion and the slow evolution of  $\text{Fe}_3\text{C}$  on the steel surface, which would not change the intrinsic rate substantially over 1 hour) compared to the galvanic current density over the same time period. The galvanic contribution in the stacked bar within Figure 8 is an average over the entire one hour time period mentioned. This figure also contains data from two repeat experiments, indicating the reproducibility of the experiments.

Figure 8 shows a clear increased contribution from the galvanic effect over time towards the total corrosion rate of the pin, corroborating the transient response from the experiment shown in Figure 7. The line graph within Figure 8 relates to the secondary axis and indicates the increase in total corrosion rate (the summation of the intrinsic corrosion rate and galvanic effect) in mm/year. An increase in total corrosion rate from ~1 to ~2.8 mm/year is observed over the course of the experiment based on the averages from repeat measurements.

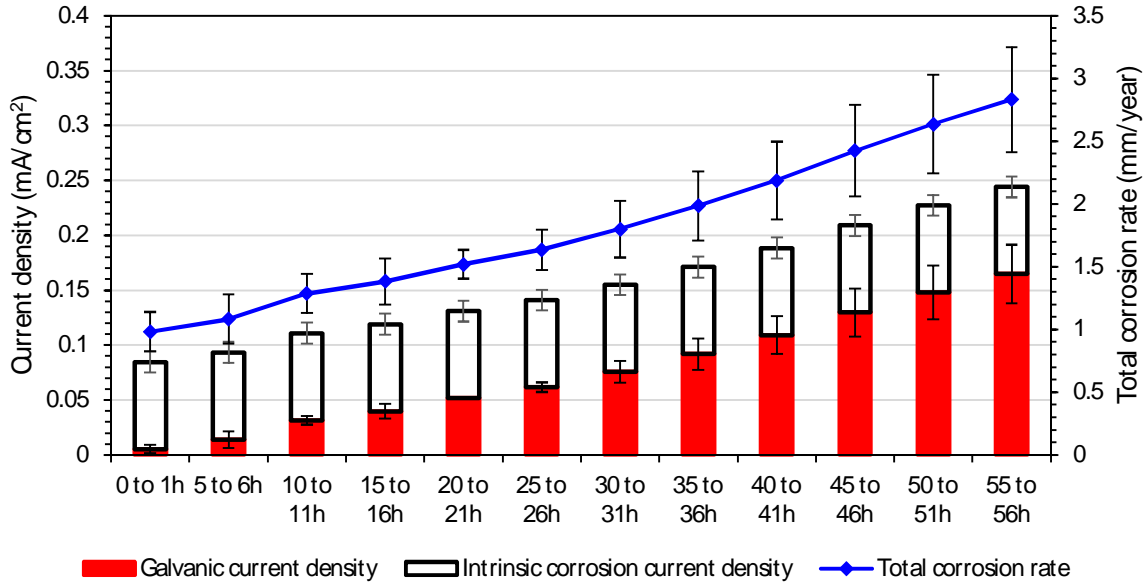


**Figure 8: Intrinsic corrosion current density of the X65 carbon steel pin at the start of each abrasion cycle compared to the average galvanic current between the large steel sample and the pin over selected 1 hour abrasion cycles (both represented as stacked bars). The line graph displays the summation of the intrinsic and galvanic values to produce a total corrosion rate for the pin over each cycle (expressed in mm/ year). Test conditions are a CO<sub>2</sub>-saturated 3.5 wt.% NaCl solution at 30°C and initial pH of 3.8 for 60 hours.**

### 3.2 Test Environment 2 – development of FeCO<sub>3</sub> film

#### 3.1.1 Corrosion rate behaviour of uncoupled sample

Figure 9 shows the corrosion rate and OCP behaviour of X65 steel over 60 hours at 70°C in a CO<sub>2</sub>-saturated 3.5 wt.% brine at pH 6.8 to 6.9. A reduction in corrosion rate is observed from ~ 1 to <0.1 mm/ year over 60 hours. The suppression in corrosion rate can be attributed to the formation of a protective FeCO<sub>3</sub> corrosion product. The ability of this corrosion product is well documented in literature in terms of its ability to significantly suppress general corrosion<sup>[31]</sup>. It has been suggested that FeCO<sub>3</sub> is able to reduce the corrosion rate by acting as a diffusion barrier and/ or blocking active sites on the steel surface through the formation of a porous crystalline structure<sup>[31]</sup>.

In contrast to the low temperature experiment where the revealing of the Fe<sub>3</sub>C layer produced a continuous increase in OCP, the potential trend in Figure 9 during the precipitation of FeCO<sub>3</sub> is more complex. The X65 steel potential reduces immediately

after being placed in the brine solution. The OCP then continues to decline as the protective film initially establishes itself, reducing from -735 mV to -745 mV as the corrosion rate drops from 1 to 0.5 mm/year over the first 8 hours.

After the 8 hour mark, the OCP begins to rise to ~ -670 mV at 30 hours in conjunction with a further decline in corrosion rate to ~ 0.1 mm/year. Beyond 30 hours, it could be argued that the OCP again drops in conjunction with a small reduction in corrosion rate, however, no significant decline in OCP is determined based on repeat measurements.

A very similar trend in the time dependence of the OCP was observed by Han et al.<sup>[1]</sup> at conditions of 80°C and pH 6.6 in a 1 wt.% NaCl solution with the addition of 50 ppm Fe<sup>2+</sup>. They reported an initial decrease in corrosion rate of 65 carbon steel over the first 3 hours of the experiment, in conjunction with a reduction in corrosion rate from 0.8 to ~0.4 mm/year. Beyond this period, the OCP began to rise by ~ 30 mV within 24 hours as the corrosion rate continued to reduce to 0.1 mm/year. The work by Han et al.<sup>[1]</sup> indicated that such OCP differences between the FeCO<sub>3</sub>-covered surface and the wet-ground steel surface resulted in the formation of galvanic cells.

The SEM image provided in Figure 10(a) and (b) show that the FeCO<sub>3</sub> crystals have covered nearly the entire steel surface. The supporting diffraction pattern from the steel surface in Figure 10(c) confirms the presence of FeCO<sub>3</sub>.

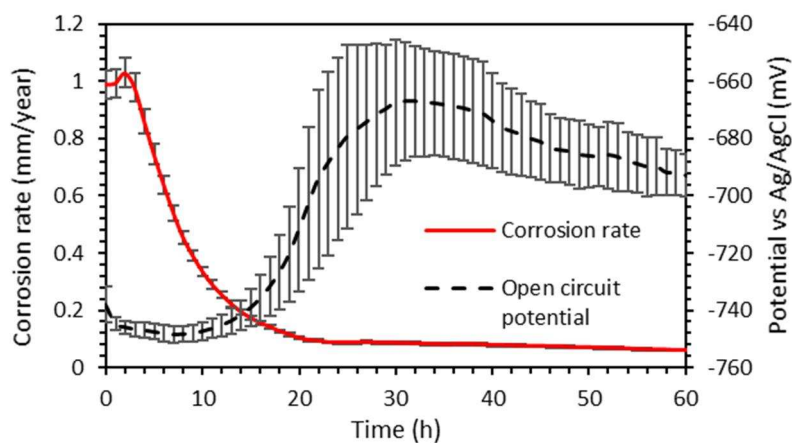
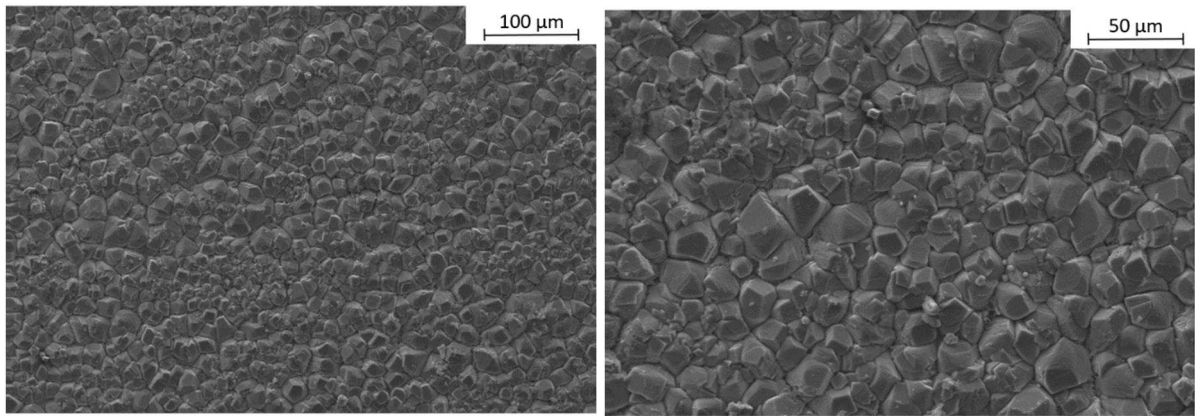
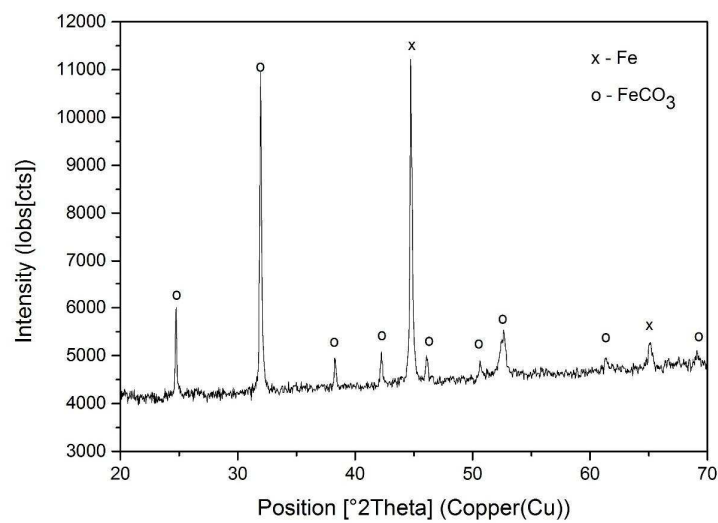


**Figure 9: Corrosion rate and open circuit potential of X65 carbon steel exposed to a CO<sub>2</sub>-saturated 3.5 wt.% NaCl solution at 70°C and pH 6.8 for 60 hours. A Stern-Geary coefficient of 17 was used to convert the charge-transfer resistance into corrosion rate.**



(a)

(b)



(c)

**Figure 10: SEM images of X65 carbon steel exposed to a CO<sub>2</sub>-saturated 3.5 wt.% NaCl solution at 70°C and pH 6.8 for 60 hours at (a) lower and (b) higher magnification, as well as (c) the corresponding diffraction pattern from the specimen surface.**

### 3.2.2 Galvanic current and mixed potential behaviour of coupled samples

Figures 11(a) to (d) show the galvanic interaction between the repeatedly abraded pin and the larger sample on which the FeCO<sub>3</sub> film is allowed to establish over 60 hours. Again, for clarity, key stages in the evolution of the mixed potential and galvanic current density between the pin and the large sample are shown over the 60 hour period in these figures.

As shown in Figure 11(a), during the early stages of the experiment, the galvanic current density exhibits a sharp drop to negative current, followed by a rise to a less negative

value for each one hour cycle. The negative current signifies that the large sample establishes itself as the net anode within the galvanic couple, resulting in the pin becoming a net cathode, causing it to corrode at a rate lower than its intrinsic corrosion rate. This behaviour is attributed to the fact that the OCP of the large sample initially drops during the early stages of the development of the  $\text{FeCO}_3$  film (as shown previously in Figure 10). Over the period shown in Figure 11(a), the average galvanic current is  $-0.028 \text{ mA/cm}^2$  which equates to a  $0.3 \text{ mm/year}$  reduction in corrosion rate for the carbon steel pin from its initial intrinsic corrosion rate of  $\sim 1 \text{ mm/year}$  in this environment. Again, over this period (and for the entire experiment for that matter), uncoupled measurements revealed that the mixed potential was dominated by that of the larger sample (in agreement with the observations of Han et al.<sup>[11]</sup>). Furthermore, it is worth noting that from uncoupled measurements, after each abrasion, the OCP of the pin was shown to revert to be within a few mV to that of the starting potential of the larger sample at the beginning of the experiment (i.e.  $\sim -740 \text{ mV}$ ). Therefore, the changes in the mixed potential relative to its starting value at 0 hours can be thought of as an indication as to the size of the potential difference between the two specimens at the start of each abrasion cycle.

After reaching a minimum value at  $\sim 8$  hours, the mixed potential begins to rise (as shown in Figure 11(b)). As the potential of the large sample rises back above that of the abraded pin ( $\sim -740 \text{ mV}$ ), there is a reversal in the direction of the galvanic current density. Consequently, the abraded pin shifts from becoming a net cathode to a net anode. These results show that the level of  $\text{FeCO}_3$  development on the steel surface plays a critical role in influencing not only the magnitude of the interaction, but the direction of the galvanic current. From the period of 14 to 19.5 hours, the average galvanic current density is  $0.001 \text{ mA/cm}^2$  ( $0.01 \text{ mm/year}$ ). Such a small current density is sensible given that the mixed potential does not deviate significantly from that of the potential at the very start of the experiment (i.e. that of the pin every time it is abraded).

As the test continues (Figure 11(c)), the mixed potential continues to rise to  $-685 \text{ mV}$ . In conjunction with this rise in potential, an increase in the current response is also observed. However, each transient cycle consists of a positive peak in current, followed by a decay to  $\sim 0 \text{ mA/cm}^2$  within the 1 hour time frame for each abrasion cycle. This shows that the  $\text{FeCO}_3$  film is able to reform relatively quickly in these particular

experiments. This is to be expected given that the brine solution has theoretically reached  $\text{FeCO}_3$  saturation, the bulk pH is high, the temperature is relatively high and the pin is being positively polarised, increasing the surface  $\text{Fe}^{2+}$  concentration. All these factors are known to encourage the growth of  $\text{FeCO}_3$ <sup>[13, 31]</sup>. Therefore, it is important to understand that changes in any of these parameters are likely to influence the kinetics of  $\text{FeCO}_3$  formation, as well as the protective properties of the layer formed, both of which will influence the transient response and the threat of localised corrosion generated through galvanic effects.

It is perhaps worth noting at this point that both Sun et al.<sup>[32]</sup> and Han et al.<sup>[1]</sup> have suggested that the level of saturation in the bulk solution plays a critical role in such transient galvanic current density responses. They suggested that the propagation of localised corrosion would only occur if the corrosion conditions fell into the so-called 'grey zone'. This region was defined as conditions where the solution was close to saturation of  $\text{FeCO}_3$ . It was assumed that when supersaturation was  $\gg 1$ ,  $\text{FeCO}_3$  would precipitate on all surfaces, resulting in the 'healing' of active localised regions. Conversely, for systems under-saturated with respect to  $\text{FeCO}_3$ , the  $\text{FeCO}_3$  film would dissolve and uniform corrosion would occur. It was believed that only at the near saturation point, that protective layers would neither be dissolved from the surface of the cathode, nor precipitation would occur on the anode, allowing a steady galvanic interaction to be maintained.

Based on this discussion from Sun et al.<sup>[32]</sup> and Han et al.<sup>[1]</sup> it could be argued that one limitation of the experimental technique performed in this study is that the level of supersaturation in the solution is not maintained throughout the course of the experiment (i.e. not analogous to one steady-state point within a carbon steel pipeline during production). Nonetheless, the technique is able to indicate how the galvanic interaction responds during the formation of an  $\text{FeCO}_3$  layer. Controlling and/or considering the brine saturation level of  $\text{FeCO}_3$  is a critical for such environments and will be the subject of future experiments, allowing the galvanic effects to be evaluated at specific fixed values of pH, temperature and  $\text{FeCO}_3$  supersaturation. Numerous authors have shown that while localised corrosion of carbon steel appears favourable in some environments, in others it does not occur<sup>[1, 2, 33, 34]</sup>. By controlling the brine chemistry more carefully in experiments such as these, it is possible to investigate such boundaries

of operation and environments conducive to localised corrosion i.e. the so-called 'grey zone'.

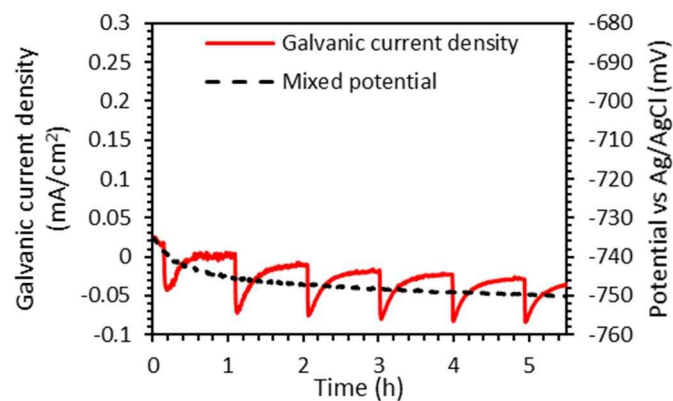
From 30 to 35.5 hours in Figure 11(c), the average galvanic current density is  $0.027 \text{ mA/cm}^2$  ( $0.31 \text{ mm/year}$ ) with a mixed potential  $\sim 45\text{-}50 \text{ mV}$  above the starting potential. Interestingly, over this period, the mixed potential is influenced by the abrasion process. This can be attributed to the fact that the suppression of the corrosion rate on the large specimen is so significant that once the pin is abraded the anodic and cathodic total currents are large enough to result in the mixed potential being influenced slightly by that of the smaller specimen.

Figure 11(d) shows that for this particular experiment, the mixed potential drops toward the end of the test to  $-700 \text{ mV}$  ( $30\text{-}35 \text{ mV}$  above the starting potential). Over this range from 50 to 55.5 hours, the average galvanic current density is  $0.023 \text{ mA/cm}^2$  ( $0.26 \text{ mm/year}$ ). Comparison between Figures 11(c) and (d) indicates that this galvanic current response is driven by the potential difference, as shown previously in experiments by Han et al.<sup>[1]</sup> i.e. a higher potential difference results in a greater magnitude in galvanic current before the 'healing' of the anodic pin. However, in this instance, the galvanic effects induced by the  $\text{Fe}_3\text{C}$  layer at low temperature appear to be far more significant than those observed in the higher temperature tests where  $\text{FeCO}_3$  precipitates. It is also important to mention that the average current densities reported for Figures 11(c) and (d) will be a strong function of the frequency of the abrasion process.

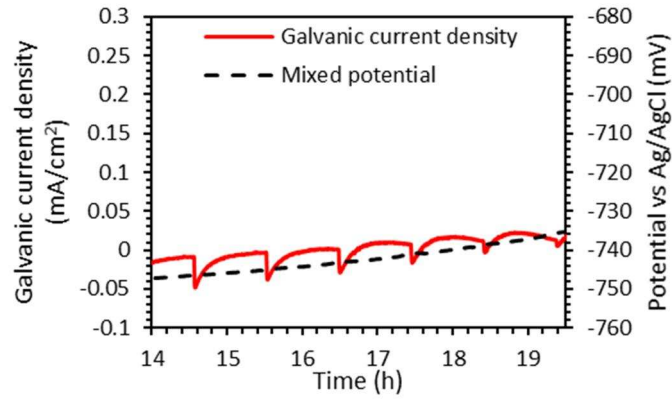
The response in Figure 11(d) relates to that encountered for a fully protective  $\text{FeCO}_3$  film, enabling the values to be compared with other studies reported in the literature focusing on the galvanic interactions produced by fully established protective layers. In a similar setup to the one conducted here, Han et al.<sup>[1]</sup> evaluated the galvanic current density exchanged between a  $16 \text{ cm}^2$  cathode ( $\text{FeCO}_3$  covered X65) and a  $0.018 \text{ cm}^2$  anode pin (bare X65 surface) over a wide range of conditions, using a pencil pit configuration with the anodic pit isolated in the centre of the cathode. Depending upon the conditions studied, the 'healing' time for the anodic pit varied significantly, ranging from  $<1$  hour (as with experiments performed here) to not fully healing at all over 100 hours. In the tests where rapid healing was observed, these were recorded in supersaturated environments

which were  $>1$ , supporting the observations in this study regarding the observed rapid healing of the anode.

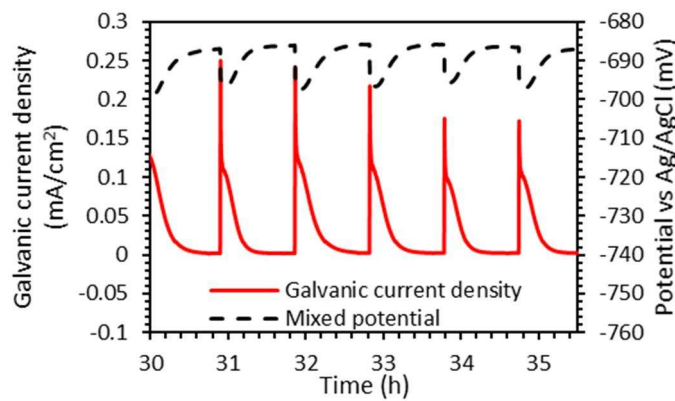
In relation to the magnitude of the galvanic current, this has been shown to be strongly dependent on the cathode to anode area ratio. This was demonstrated by Fernandez-Domene et al.<sup>[21]</sup> in which different areas of the  $\text{FeCO}_3$  covered cathode were connected to a fixed area bare steel anode, resulting in area ratios ranging from 1:1 up to 200:1 for the cathode to anode ratio, respectively. Tests were conducted in a  $\text{CO}_2$ -saturated solution at  $60^\circ\text{C}$  and pH 5.5, therefore the process of anode 'healing' was particularly slow. The results showed that as the area ratio increased from 1:1 to 200:1, so too did the galvanic current from  $3.8 \pm 0.12$  to  $263 \pm 43 \mu\text{A}/\text{cm}^2$  ( $0.0038$  to  $0.263 \text{ mA}/\text{cm}^2$ ). Comparing to the results in this work (where the area ratio is  $\sim 150:1$ ), the reported galvanic currents agree well with the peak current densities of between  $0.05$  and  $0.15 \text{ mA}/\text{cm}^2$  shown in Figures 11(c) and (d). However, the rate of diminution in the experiments is far faster here due to the difference in operating conditions. As suggested through the work of Han et al.<sup>[1]</sup>, the rate of reduction in galvanic current will be sensitive to temperature, pH and bulk/surface  $\text{FeCO}_3$  saturation, with increases in all the aforementioned properties inducing faster reductions in galvanic current.



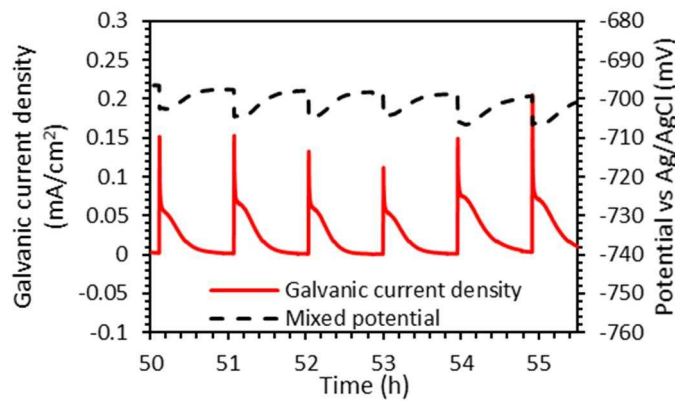
(a)



(b)



(c)



(d)

**Figure 11: Galvanic current and mixed potential as a function of time for an X65 steel pin connected to a larger X65 sample, where the steel pin is abraded repetitively every hour for 3 seconds and the large sample is left to corrode. Test conditions are a CO<sub>2</sub>-saturated 3.5 wt.% NaCl solution at 70°C and pH 6.8 for 60 hours; (a) time period of 0 to 5.5 hours; (b) time period of 14 to 19.5 hours; (c)**

**time period of 30 to 35.5 hours and (d) time period of 50 to 55.5 hours displayed for clarity.**

Figure 12 shows the intrinsic corrosion rate of the pin at the very beginning of selected one-hour time periods compared to the average galvanic current density over the same selected time intervals. Given that the diminution in galvanic current in each cycle is associated with protective  $\text{FeCO}_3$  formation, (resulting in suppression of the intrinsic corrosion rate over each cycle), the values shown in Figure 12 for the intrinsic corrosion current density are overestimated somewhat in terms of the entire 1 hour cycle. However, the results can be thought of as a worst-case scenario by utilising these values, as well as providing an indication of the relative size of the galvanic effect compared to the initial intrinsic corrosion behaviour of a bare steel surface over each time interval. As in Figure 8, the line graph provides the total corrosion rate based on the summation of the two components and is expressed in mm/year, relating to the secondary y-axis.

Figure 12 shows that the total corrosion rate of the pin is suppressed by the galvanic effect induced during the earlier stages of  $\text{FeCO}_3$  development on the larger sample (as the OCP drops below the initial starting value (shown previously in Figure 9)). As the OCP rises from ~10h onwards and the corrosion rate response of the large sample plateaus at a low value, the average galvanic contribution over each cycle also rises before stabilising at ~0.03 mA/cm<sup>2</sup>. This results in the total corrosion rate of the pin stabilising at ~1.4 mm/year (assuming a constant intrinsic corrosion rate of ~1 mm/year over the entire 1 hour cycle as a worst case scenario).

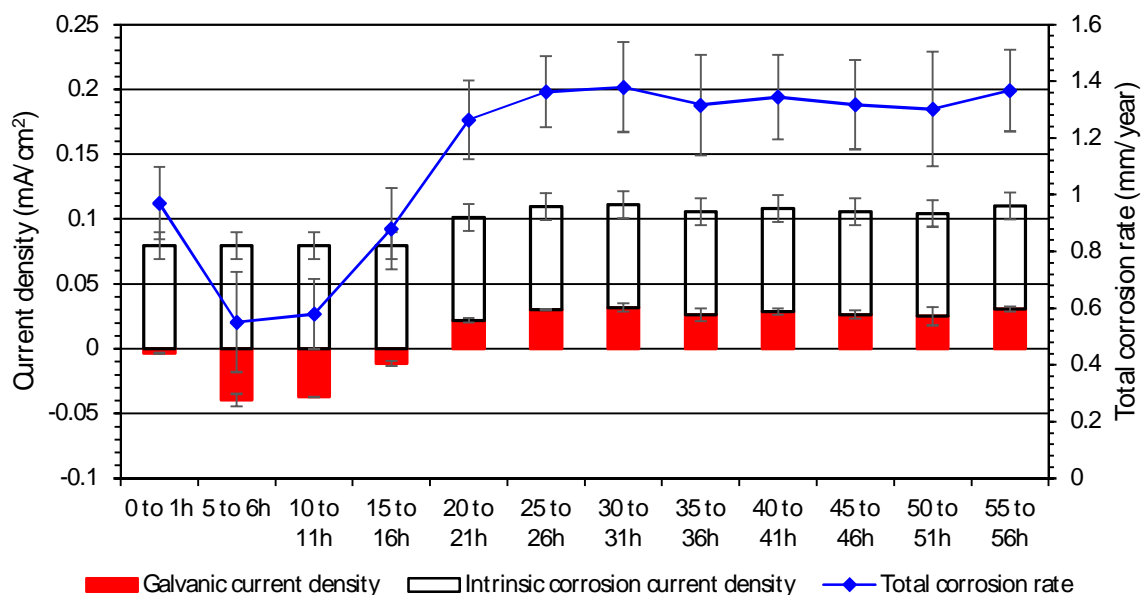


**Figure 12: Intrinsic corrosion current density of the X65 carbon steel pin at the start of each abrasion cycle compared to the average galvanic current between the large steel sample and the pin over selected 1 hour abrasion cycles (both represented as stacked bars). The line graph displays the summation of the intrinsic and galvanic values to produce a total corrosion rate for the pin over each cycle (expressed in mm/ year). Test conditions are a CO<sub>2</sub>-saturated 3.5 wt.% NaCl solution at 70°C and pH 6.8 for 60 hours.**

#### **4.0 Conclusions**

This paper focuses on the design and preliminary testing of an automated underwater abrasion rig to assist in understanding the galvanic interaction induced by surface films when continuous localised mechanical film breakdown is encountered on the surface of carbon steel in CO<sub>2</sub>-containing environments. The rig is used to look at the evolution and galvanic interactions which exist in two model environments where either Fe<sub>3</sub>C or FeCO<sub>3</sub> are the dominant corrosion products on the steel surface. From the study, the following conclusions can be made:

- The designed rig is able to produce repeatable results which reveal information relating to the galvanic interaction on steel surfaces which are largely covered with surface films/ corrosion products but have local disruptions where the surface films are removed i.e. analagous to a tribo-corrosion process where local removal of material occurs within a carbon steel pipeline as a result of periodic sand particle impingement.
- The revealing of a Fe<sub>3</sub>C layer on the larger steel specimen (4.9 cm<sup>2</sup>) at 30°C and pH 3.8 resulted in an increase in both corrosion rate and OCP over 60 hours, which was attributed to the ability of Fe<sub>3</sub>C to support the hydrogen evolution reaction in a CO<sub>2</sub> environment.
- ZRA coupling of the large specimen with the Fe<sub>3</sub>C-rich layer to a small X65 sample which was repeatedly abraded resulted in a the small sample establishing itself as a net anode. This indicated that the bare steel was susceptible to accentuated corrosion rates due to the galvanic effects induced from the Fe<sub>3</sub>C covered surface. The galvanic interaction increased concomitantly with the potential of the larger sample (i.e. the potential difference between the two samples), accentuating the

corrosion rate of the small sample to ~3.4 mm/year after 60 hours, which was three times that of the intrinsic corrosion rate.

- The precipitation of a  $\text{FeCO}_3$  layer on the larger steel specimen at 70°C and pH 6.8 resulted in a diminution in corrosion rate over 60 hours from 1 to 0.1 mm/year, with OCP initially falling within the first 8 hours, before rising to more noble values.
- Galvanic coupling to the abraded pin resulted in the small sample acting as a net cathode when the potential of the large sample fell below the starting potential in the early stages of film development. However, as the  $\text{FeCO}_3$  film evolved on the large sample, the rise in potential created a reversal in polarity, turning the small pin into the net anode. The galvanic interactions were not as significant as those observed at lower temperature with  $\text{Fe}_3\text{C}$ , however, this was attributed to the favourable condition for rapid formation and 'healing' of the abraded pin compared to the slow revealing of  $\text{Fe}_3\text{C}$  in the lower temperature environment.
- The system provides an effective form of measurement to determine how galvanic interactions evolve during the development of surface films. The system has the potential to be extended to hydrogen sulphide environments to consider the effects of transition in iron sulphide films over long durations, as well as the behaviour of corrosion inhibitors and passive materials in oil and gas environments.

## 5.0 References

1. J Han, B.N. Brown, and S. Nešić, "Investigation of the galvanic mechanism for localized carbon dioxide corrosion propagation using the artificial pit technique", *Corrosion*, 66, 9 (2010): p. 1-12.
2. F. Pessu, R. Barker, and A. Neville, "The influence of pH on localized corrosion behavior of X65 carbon steel in  $\text{CO}_2$ -saturated brines", *Corrosion*, 71, 12 (2015): p. 1452-1466.
3. F. Pessu, R. Barker, and A. Neville, "Understanding pitting corrosion behavior of X65 carbon steel in  $\text{CO}_2$ -saturated environments: The temperature effect", *Corrosion*, 72, 1 (2015): p. 78-94.
4. F. Pessu, R. Barker, and A. Neville, "Pitting and uniform corrosion of X65 carbon steel in sour corrosion environments: the influence of  $\text{CO}_2$ ,  $\text{H}_2\text{S}$ , and temperature", *Corrosion*, 73, 9 (2017): p. 1168-1183.
5. F. Pessu, Y. Hua, R. Barker, and A. Neville, "A study of the pitting and uniform corrosion characteristics of X65 carbon steel in different  $\text{H}_2\text{S}$ - $\text{CO}_2$ -containing environments", *Corrosion*, 74, 8 (2018): p. 886-902.

6. J Amri, E. Gulbrandsen, and R. Nogueira, "The effect of acetic acid on the pit propagation in CO<sub>2</sub> corrosion of carbon steel", *Electrochemistry Communications*, 10, 2 (2008): p. 200-203.
7. J Amri, E. Gulbrandsen, and R. Nogueira, "Pit growth and stifling on carbon steel in CO<sub>2</sub>-containing media in the presence of HAc", *Electrochimica Acta*, 54, 28 (2009): p. 7338-7344.
8. W. Lee, Z. Lewandowski, P.H. Nielsen, and W.A. Hamilton, "Role of sulfate-reducing bacteria in corrosion of mild steel: A review", *Biofouling*, 8, 3 (1995): p. 165-194.
9. J Crolet, N. Thevenot, and S. Nešić, "Role of conductive corrosion products in the protectiveness of corrosion layers", *Corrosion*, 54, 3 (1998): p. 194-203.
10. R. Barker, D. Burkle, T. Charpentier, H. Thompson, and A. Neville, "A review of iron carbonate (FeCO<sub>3</sub>) formation in the oil and gas industry", Submitted to *Corrosion Science*, (2018).
11. M. Kermani and A. Morshed, "Carbon dioxide corrosion in oil and gas production - A compendium", *Corrosion*, 59, 8 (2003): p. 659-683.
12. S. Nesic, N. Thevenot, J-L. Crolet, and D. Drazic. "Electrochemical properties of iron dissolution in the presence of CO<sub>2</sub>-Basics revisited", *CORROSION 96*, paper no. 96003, (Houston, TX:NACE, 1996).
13. R. Barker, Y. Hua, and A. Neville, "Internal corrosion of carbon steel pipelines for dense-phase CO<sub>2</sub> transport in carbon capture and storage (CCS)—a review", *International Materials Reviews*, 62, 1 (2017): p. 1-31.
14. A. Dugstad. "The importance of FeCO<sub>3</sub> supersaturation on the CO<sub>2</sub> corrosion of mild steels", *CORROSION 92*, paper no. 92014, (Houston TX: NACE, 1992).
15. S. Nesic, J Lee, and V. Ruzic. "A mechanistic model of iron carbonate film growth and the effect on CO<sub>2</sub> corrosion of mild steel", paper no. 02237, (Denver, CO:NACE, 2002).
16. E. Van Hunnik, E. Hendriksen, and B.F. Pots. "The formation of protective FeCO<sub>3</sub> corrosion product layers in CO<sub>2</sub> corrosion", *CORROSION 96*, paper no. 96006, (Denver, CO: NACE International Conference, 1996).
17. K. Videm and A. Dugstad. "Film covered corrosion, film breakdown and pitting attack of carbon steels in aqueous CO<sub>2</sub> environments", *CORROSION 88*, paper no. 88186, (Houston, TX: NACE, 1988).
18. V. Ruzic, M. Veidt, and S. Nešić, "Protective iron carbonate films-Part 1: Mechanical removal in single-phase aqueous flow", *Corrosion*, 62, 5 (2006): p. 419-432.
19. V. Ruzic, M. Veidt, and S. Nešić, "Protective iron carbonate films-Part 3: Simultaneous chemo-mechanical removal in single-phase aqueous flow", *Corrosion*, 63, 8 (2007): p. 758-769.
20. V. Ruzic, M. Veidt, and S. Nešić, "Protective iron carbonate films-Part 2: Chemical removal by dissolution in single-phase aqueous flow", *Corrosion*, 62, 7 (2006): p. 598-611.
21. R.M. Fernández-Domene, J Andrews, R. Leiva-García, and R. Akid. "Galvanic Corrosion Following Local Breakdown of a Scale Formed on X-65 in CO<sub>2</sub> Saturated Solutions", *CORROSION 2015: NACE International*, (2015).

22. JW. Palmer, J Marsh, and R.C. Newman. "Evaluation of Inhibitor Performance for Protection against Localized Corrosion", CORROSION 2002, (Denver, Colorado: NACE International, 2002).
23. A. Turnbull, D. Coleman, A. Griffiths, P. Francis, and L. Orkney, "Effectiveness of corrosion inhibitors in retarding the rate of propagation of localized corrosion", Corrosion, 59, 3 (2003): p. 250-257.
24. JW. Martin and A.J McMahon. "Simulation Tests On The Effects Of Mechanical Damage 0 Acid Cleaning On Corrosion Resistant Alloys Used For Oil/ Gas Production Well Tubulars", CORROSION 2004, (New Orleans, Louisiana: NACE International, 2004).
25. H.E. Rincon, JR. Shadley, K.P. Roberts, and E.F. Rybicki. "Erosion-Corrosion Of Corrosion Resistant Alloys Used In The Oil And Gas Industry", CORROSION 2008, (New Orleans, Louisiana: NACE International, 2008).
26. H. Rincon, JR. Shadley, and E.F. Rybicki. "Erosion Corrosion Phenomena of 13Cr at Low Sand Rate Levels", CORROSION 2005, (Houston, Texas: NACE International, 2005).
27. F. Farelas, M. Galicia, B. Brown, S. Nešić, and H. Castaneda, "Evolution of dissolution processes at the interface of carbon steel corroding in a CO<sub>2</sub> environment studied by EIS", Corrosion Science, 52, 2 (2010): p. 509-517.
28. F. Farelas, B. Brown, and S. Nešić. "Iron carbide and its influence on the formation of protective iron carbonate in CO<sub>2</sub> corrosion of mild steel", CORROSION 2013, paper no. 2291, (Orlando, FL: NACE, 2013).
29. JL. Mora-Mendoza and S. Turgoose, "Fe<sub>3</sub>C influence on the corrosion rate of mild steel in aqueous CO<sub>2</sub> systems under turbulent flow conditions", Corrosion Science, 44, 6 (2002): p. 1223-1246.
30. R. Barker, X. Hu, A. Neville, and S. Oushnaghan. "Assessment of Preferential Weld Corrosion of Carbon Steel Pipework In CO<sub>2</sub>-Saturated Flow-Induced Corrosion Environments": NACE International, 2012).
31. R. Barker, D. Burkle, T. Charpentier, H. Thompson, and A. Neville, "A review of iron carbonate (FeCO<sub>3</sub>) formation in the oil and gas industry", Corrosion Science, (2018).
32. Y. Sun, K. George, and S. Nestic, "The effect of Cl- and acetic acid on localized CO<sub>2</sub> corrosion in wet gas flow", CORROSION 2003, (2003).
33. J Shadley, S. Shirazi, E. Dayalan, M. Ismail, and E. Rybicki, "Erosion-corrosion of a carbon steel elbow in a carbon dioxide environment", Corrosion, 52, 9 (1996): p. 714-723.
34. R. Nyborg and A. Dugstad. "Mesa corrosion attack in carbon steel and 0.5% chromium steel", CORROSION 98, paper no. 98029, (San Diego, CA: NACE, 1998).